Atmos. Chem. Phys., 6, 35–49, 2006
www.atmos-chem-phys.org/acp/6/35/
SRef-ID: 1680-7324/acp/2006-6-35
European Geosciences Union

Atmospheric Chemistry and Physics

The initial dispersal and radiative forcing of a Northern Hemisphere mid-latitude super volcano: a model study

C. Timmreck[1] **and H.-F. Graf**[1,2]

[1]Max-Planck Institut für Meteorologie, Hamburg, Germany
[2]Centre for Atmospheric Science University of Cambridge, UK

Received: 19 May 2005 – Published in Atmos. Chem. Phys. Discuss.: 22 August 2005
Revised: 7 November 2005 – Accepted: 27 November 2005 – Published: 4 January 2006

Abstract. The chemistry climate model MAECHAM4/CHEM with interactive and prognostic volcanic aerosol and ozone was used to study the initial dispersal and radiative forcing of a possible Northern Hemisphere mid-latitude super eruption. Tropospheric climate anomalies are not analysed since sea surface temperatures are kept fixed. Our experiments show that the global dispersal of a super eruption located at Yellowstone, Wy. is strongly dependent on the season of the eruption. In Northern Hemisphere summer the volcanic cloud is transported westward and preferentially southward, while in Northern Hemisphere winter the cloud is transported eastward and more northward compared to the summer case. Aerosol induced heating leads to a more global spreading with a pronounced cross equatorial transport. For a summer eruption aerosol is transported much further to the Southern Hemisphere than for a winter eruption. In contrast to Pinatubo case studies, strong cooling tendencies appear with maximum peak values of less than -1.6 K/day three months after the eruption in the upper tropical stratosphere. This strong cooling effect weakens with decreasing aerosol density over time and initially prevents the aerosol laden air from further active rising. All-sky net radiative flux changes of less than -32 W/m^2 at the surface are about a factor of 6 larger than for the Pinatubo eruption. Large positive flux anomalies of more than 16 W/m^2 are found in the first months in the tropics and sub tropics. These strong forcings call for a fully coupled ocean/atmosphere/chemistry model to study climate sensitivity to such a super-eruption.

Correspondence to: C. Timmreck
(timmreck@dkrz.de)

1 Introduction

While there is an increasing number of publications on the climate effects of large volcanic eruptions like Mt. Pinatubo in 1991, there is very little known for the extreme eruptions that are rare events in Earth history but have a large risk potential. Super eruptions are defined to be those eruptions yielding in excess of 10^{15} kg of products (volatile gases (mainly SO_2 and H_2O) and ash particles) with a volcanic explosivity index (VEI) of 8 or larger (Mason et al., 2004). A VEI 8 is estimated to release about 1000 Mt SO_2 (Rampino, 2002). SO_2, which is mainly responsible for the climatic effects of explosive volcanic eruptions, is transferred to sulphate aerosol by chemical reactions. Volcanic sulphate aerosols have a strong influence on the atmospheric system by changing its chemical composition and by altering its radiation balance. The scattering of incoming solar radiation back to space (direct effect) leads to cooling at the surface and counteracts the greenhouse effect. The additional aerosol loading further increases the temperature in the aerosol containing layers through the absorption of near infrared and long wave radiation.

Previous work in the field of volcanic radiative forcing calculations mainly addressed tropical volcanoes. Several studies were published about the radiative effects of the 1991 Pinatubo eruption (e.g., Kinne et al., 1992; Stenchikov et al., 1998; Andronova et al., 1999; Ramachandran et al., 2000). While in most papers the aerosol distribution and radiative properties are derived from observations, Timmreck et al. (1999a, 1999b) transported the Pinatubo aerosol and coupled it directly with the radiation scheme of the ECHAM GCM, emphasising the importance of an interactive treatment of the volcanic cloud for the initial transport. Several model studies are available in the literature concerning the effects of tropical volcanoes of the size of the Mt. Pinatubo June 1991 eruption on climate (e.g., Hansen et al., 1992;

Graf et al., 1993; Kirchner et al., 1999; Stenchikov et al., 2002; Yang and Schlesinger, 2002) but only very few for mid-latitude eruptions of the same size are published (e.g., Graf and Timmreck, 2001). In the case of the Laacher See eruption (10 900 B.C.) Graf and Timmreck (2001) found that the volcanic aerosol was clearly restricted to the Northern Hemisphere leading to strong stratospheric cooling due to intensified long wave emission in the polar night and to an intensified polar vortex.

Studies of atmospheric effects of super-eruptions (i.e. such events which are extremely rare and include prehistoric events like Toba (74 000 years ago, Oppenheimer, 2002) or the Yellowstone eruptions, the last of which took place ca. 639 000 years before present (Smith and Siegel (2000); Lanphere et al. (2002)), were covered only by very few publications (e.g. Bekki et al., 1996). In general, it is speculated that these eruptions would have lead to massive cooling globally lasting for several years. However, the effects of volcanic aerosols on climate seem to be highly dependent upon whether or not they are trapped at high latitudes or are allowed to spread globally. Thus, it is worthwhile to investigate the initial transport path of the cloud dependent on the season of the eruption. This could be important at higher latitudes where strong westerly winds exist in winter and weak easterlies in summer.

In this study we investigate this problem using the chemistry climate model MAECHAM4/CHEM with interactive and prognostic volcanic aerosol and ozone (Timmreck et al., 2003) to study a possible Northern Hemisphere mid-latitude super eruption in different times of the year. We will focus on the initial dispersal and radiative forcing of the volcanic sulphate aerosol in the first year after the eruption, but we will also address dynamical and chemical changes. Tropospheric climate sensitivity is not studied since sea surface temperatures are kept fixed and the simulation period is relatively short. We choose for our study the geographical location of the Yellowstone National Park because it seems to be one of the most likely possible sites for such an event at higher latitudes nowadays. Due to its proximity to the stratospheric Aleutian high the chance of seasonal dependence on the dispersion of the aerosols is greatest.

Important parameters for climate studies (e.g. sulphur emission, eruption height) of the past super eruptions are unknown. In the case of our mid-latitude study we choose therefore parameters which have been observed after the Pinatubo eruption, the largest eruption of the 20th century. As erupted material other than SO_2 has a much smaller atmospheric life time and a smaller atmospheric radiative effect, we concentrate on the SO_2 emission assuming an initial volcanic cloud mass of 1700 Mt SO_2, i.e. 100 times the strength of the Pinatubo eruption. An injected mass of SO_2 yields a sulfuric acid aerosol of 3470 Mt H_2SO_4/H_2O (75%)) which is in the middle of the estimated range (2300–4700 Mt) for the Younger Toba Tuff eruption, the largest known Quaternary eruption (Oppenheimer, 2002). With our study we want to add some arguments to the discussion in terms of initial aerosol radiative forcing, based on a state of the art model.

2 Experiment description

2.1 Model set-up

The chemistry climate model MAECHAM4/CHEM (Steil et al., 2003; Manzini et al., 2003) extends with 39 layers from the surface to 0.01 hPa. The prognostic variables are vorticity, divergence, surface pressure, temperature, water vapour, and cloud (liquid and ice) water content. The MAECHAM4/CHEM is run at T30 resolution. Physical processes and nonlinear terms of dynamical fields are calculated on a Gaussian longitude-latitude grid with a nominal resolution of $3.75° \times 3.75°$. The chemistry scheme describes stratospheric O_3 and tropospheric background NO_x-HO_x-CH_4-CO-O_3 chemistry. 18 variables are transported, while family members and radicals are calculated analytically. 110 photochemical reactions and heterogeneous reactions on polar stratospheric clouds and sulfate aerosols are considered. For the current study, a tropospheric sulphur scheme (Feichter et al., 1996) is coupled to the MAECHAM4/CHEM. The sulfur scheme calculates transport, emission, chemistry and wet and dry deposition of DMS, SO_2 and SO_4^{2-}. It has been suggested (Pinto et al., 1989; Bekki, 1995) that for extremely large volcanic eruptions the stratospheric OH concentration can be significantly reduced by the SO_2 oxidation and the troposphere can be shielded from the UV flux. This implies a prolonged SO_2 lifetime and therefore a longer volcanic perturbation. These effects have not been taken into account in the current study where we concentrate on the initial dispersal of the volcanic cloud. In analogy to Timmreck et al. (2003) the H_2O/H_2SO_4 aerosol is considered by a bulk approach and a simple parametrisation for the aerosol size distribution. To keep track of the time evolution of the aerosol size distribution, we calculate the aerosol mode radius r_m from the effective radius r_e and the standard deviation of the size distribution σ. σ=1.86 is kept constant in time and space because the aerosol radiative properties are only weakly dependent on σ (Stenchikov et al., 1998). The effective radius is derived from the online calculated aerosol volume according to an empirical formula, which has been derived from aerosol size distribution measurements made at Laramie, Wy. after Pinatubo (Grainger et al., 1995). While this might not lead to optimal results under the condition of massive SO_2 injection into the stratosphere, it may serve as a first order approximation. A more sophisticated treatment needs a coupled chemistry-microphysics approach (Timmreck , 2001) that is currently prepared. The sulphate aerosol is coupled with the radiation and the chemistry scheme. The MAECHAM4 radiation scheme is based on a two–stream method with two spectral intervals in the solar and near infrared (0.25–4 μm)

(Morcrette, 1991) and six in the terrestrial part (4–250 μm) of the spectrum (Fouquart and Bonnel, 1980). It considers the absorption of greenhouse gases as well as scattering and absorption by clouds and aerosols (Roeckner et al., 1996). For the radiation calculations the volcanic aerosol optical parameters are derived from the time dependent aerosol mass mixing ratio and size and weight percentage dependent normalised extinction and absorption coefficients, and asymmetry factors. In the chemistry scheme the volcanic aerosol is considered in the calculation of heterogeneous reactions on the surface of the aerosol particles and in the calculation of the actinic flux. For a detailed model description see Timmreck et al. (2003).

2.2 Initialization of the super eruption

We assumed an initial volcanic SO_2 emission of 1700 Mt. Ash is not considered in the model although it may change the initial heating and transport. The volcanic cloud is implemented at the geographical location of Yellowstone National Park. In the horizontal the SO_2 cloud is initialised over 2 grid boxes between 40.82° N–48.24° N and 112.5° W–108.5° W. In the vertical, the initial SO_2 mass is distributed over four model layers between 47—15 hPa (21.5–29 km) with two thirds of the mass between 23–27 km. This corresponds to satellite observations after the Pinatubo eruption, which have shown that the volcanic plume reached up to a height of 35–40 km, with the bulk of the aerosol centred around 25 km and ranging between 20 km and 29 km (Sparks et al., 1997). It is worth to note that a super eruption may inject SO_2 considerably higher. The injection height will depend on the ash/gas mass flux, which, if exceeding a critical threshold, will lead to a collapse of the Plinian plume, to pyroclastic flows and secondary eruption plumes. However, there is not enough information at this time to consistently change these initial conditions and thus we propose a generic super eruption.

To study the seasonally dependent transport we have carried out two experiments for typical months of Northern Hemisphere summer and winter circulation. In the first one the volcanic cloud is released in mid June (YESTJUN), in the second one the volcanic cloud is released in mid December (YESTDEC). The experiments are performed under present day conditions with chemical emissions from 1990 (Steil et al., 2003). The sea surface temperature (SST) is prescribed by monthly mean data using the AMIP dataset (Gates et al., 1999). In the following we will consider only the first 12 months after the eruption, when the impact on slower components of the climate system (ocean and biosphere) is small. For a longer simulation period it is expected that the the feedback on the OH concentration and various climate feedbacks (response of the ocean and biosphere) will become more and more important. Such simulation is planned for the near future and requires dynamic coupling of ocean and vegetation.

3 Results

3.1 Global dispersal of the volcanic cloud

The global spreading of the aerosol cloud is an essential element of a fully interactive super volcano simulation. In Fig. 1, the spatio-temporal development of the simulated aerosol column burden is shown for both experiments for the first two weeks after the eruption. The initial dispersal of the volcanic cloud is completely different between both experiments. In the summer case, YESTJUN, the volcanic cloud moves west and preferentially southward. In the winter case, YESTDEC, the simulated volcanic cloud rapidly moves east- and more northward compared to YESTJUN. Similar as was observed for the Pinatubo eruption, the volcanic cloud has encircled the earth after two weeks in both experiments. However, the aerosol cloud in YESTDEC remains in the Northern Hemisphere while in YESTJUN a significant portion of the aerosol has crossed the equator.

While the initial dispersal of the volcanic cloud in YESTDEC is similar to what one would anticipate from other Northern Hemisphere volcanic simulations (Graf and Timmreck, 2001), the transport characteristic of the volcanic cloud in YESTJUN is different. Reason for this significant difference is the Aleutian high, which in the summer months drives the volcanic cloud towards the equator. In winter strong westerly winds are predominant which transport air east and polewards. The different transport characteristics of the volcanic cloud in both experiments is also mirrored in the attached movies where the global dispersal of the aerosol mixing ratio at 24 km is shown for the first year after the eruption (Movie 1 and 2 (see supplement: http://www.atmos-chem-phys.org/acp/6/35/acp-6-35-sp.zip) and in the zonal mean optical depth $\tau_{0.5}$ (Fig. 2). Optical depths exceeding $\tau_{0.5}$=5 at λ=0.5 μm are found in YESTJUN during the first 6 months after the eruption predominantly between 5° S–50° N. Further poleward transport is reduced in the Northern Hemisphere winter stratosphere by the developing polar vortex, which represents an efficient boundary for trace species. In the winter scenario the volcanic aerosol is more confined to the Northern Hemisphere. Maximum optical depth exceeding $\tau_{0.5}$=5 is found between 20° N–60° N. In the Southern Hemisphere the optical depth is much less increased than in YESTJUN. Optical depths of $\tau_{0.5}>2.5$ are not reached in YESTDEC south of 5° S while in YESTJUN this value is reached, in the first half year after the eruption, even in the Southern Hemisphere mid-latitudes. One year after the eruption the optical depth is still above $\tau_{0.5}$=0.5 over large areas in both experiments which corresponds to the maximum optical depth after the Pinatubo eruption. One has to keep in mind that the life time of the volcanic aerosol will probably be prolonged due to reduced SO_2 oxidation as discussed for the Toba eruption by Bekki et al. (1996). This could also modify the timing and the amount of the aerosol maximum.

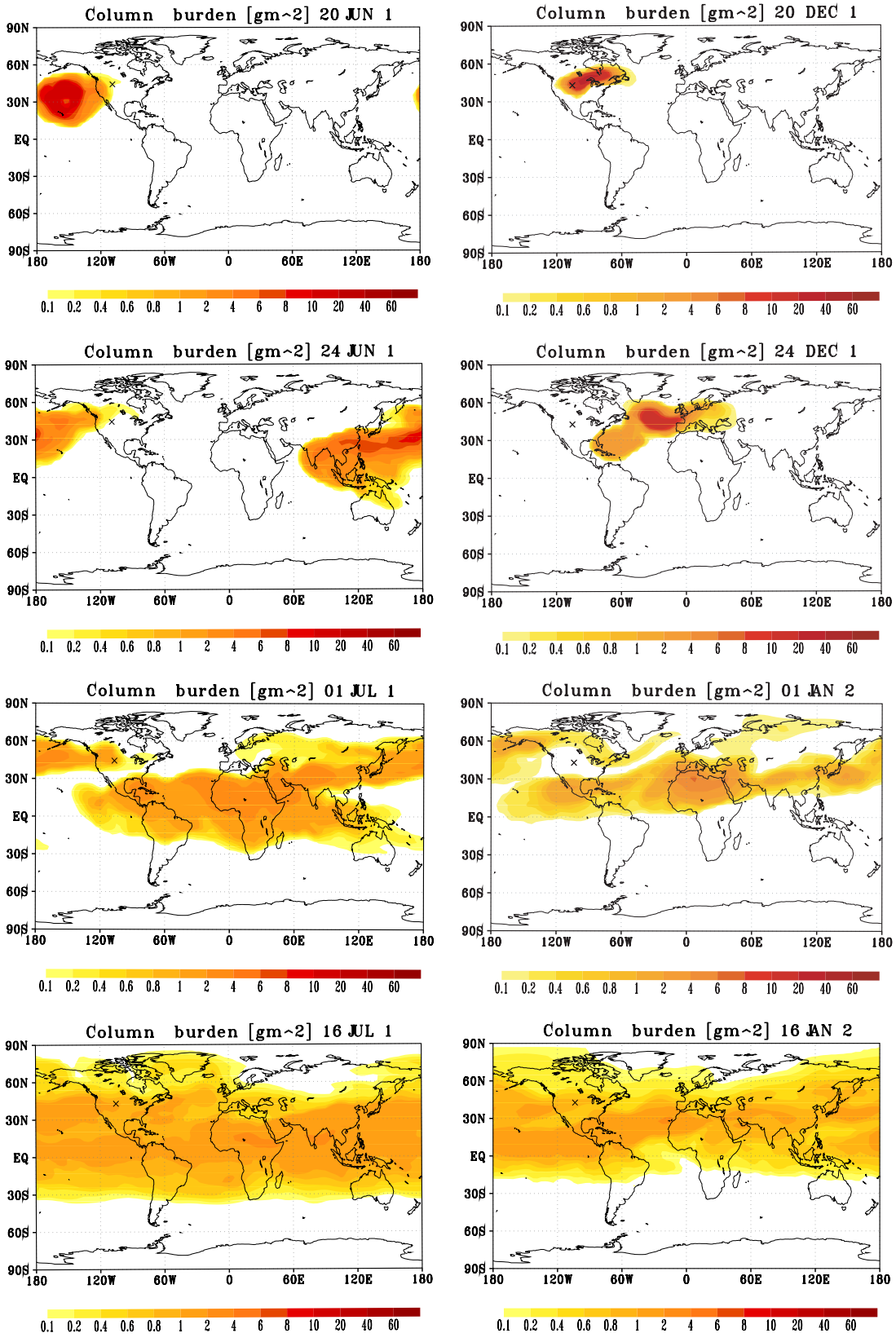

Fig. 1. Geographical distribution of aerosol column burden in both experiments for the first month after the eruption. The location of the Yellowstone National park is indicated by a cross.

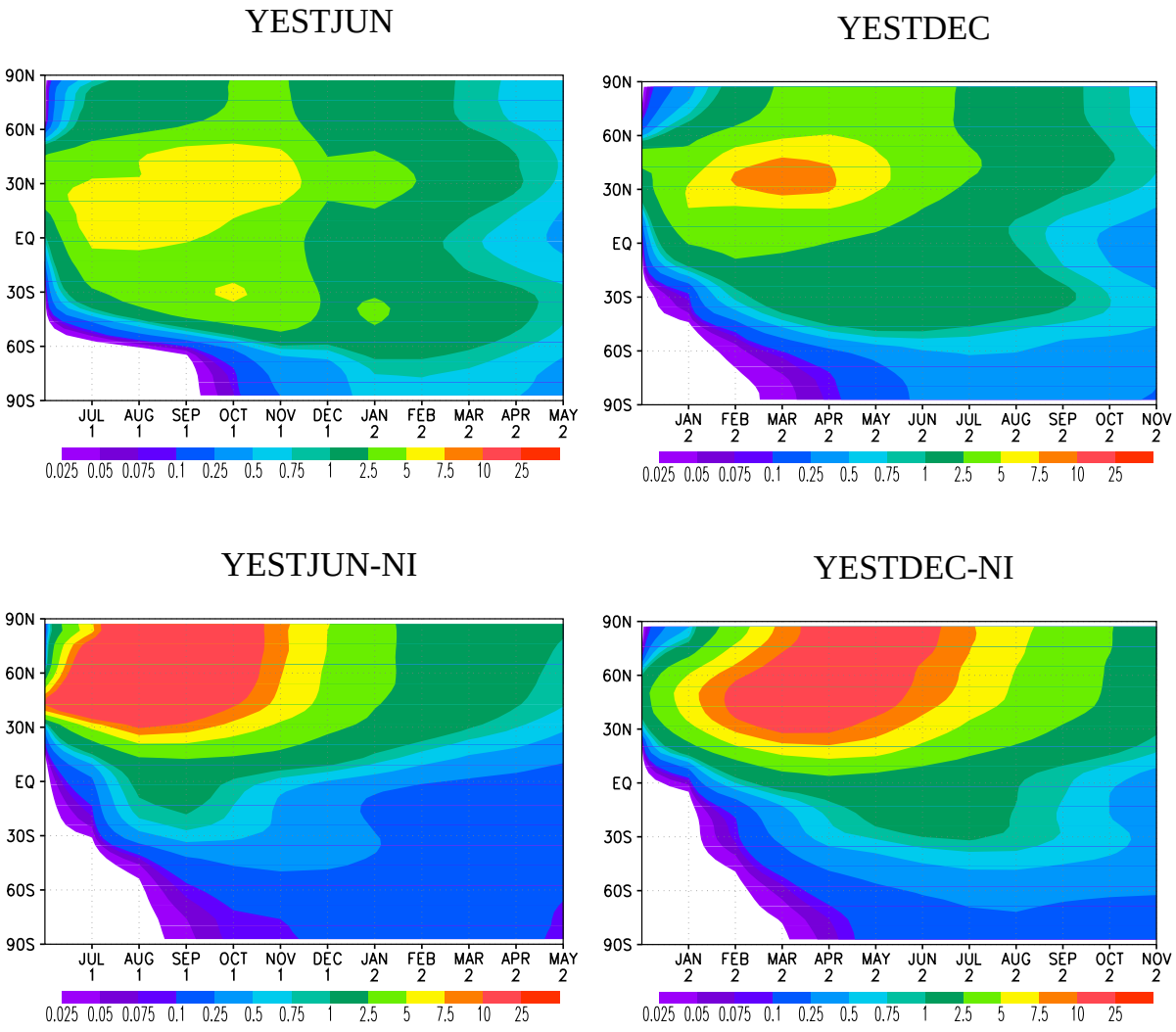

Fig. 2. Optical depth at 0.5 μm for the four experiments. The top panels show the experiments where the aerosol is treated interactivly the lower panels the corresponding non-interactive experiments. Numbers at the abscissae indicate month and year after the eruption.

The optical depth pattern looks completely different from the one which was found for the much weaker Northern Hemisphere mid-latitude volcano Laacher See eruption (Graf and Timmreck, 2001), where the aerosol was confined in Northern Hemisphere mid and high latitudes and did not reach the Southern Hemisphere. One reason for these differences is the geographical location of both volcanoes. The Laacher See is situated at Western Germany, while our theoretical super volcano is located at Yellowstone on the North American continent. The latter is, as discussed above, strongly influenced by the Aleutian high, which drives the volcanic cloud towards the equator in the summer months. Another aspect is the amount of SO_2 released: 1700 Mt for "Yellowstone" compared to 15 Mt for Laacher See. This leads to a stronger radiative forcing in the super volcano case which will discussed below.

3.2 Influence of radiative heating on the initial transport

Previous model studies for the Mt. Pinatubo aerosol (Young et al., 1994; Fairlie, 1995; Timmreck et al., 1999b) stressed the importance of the locally induced aerosol heating for the equatorial displacement of the volcanic cloud. We therefore set up two experiments (YESTJUN-NI – analogous to YESTJUN and YESTDEC-NI analogous to YESTDEC), where the volcanic aerosol is not treated interactively, but is only passively transported. Similar to YESTJUN and YESTDEC the initial volcanic cloud is transported westward in YESTJUN-NI and eastward in YESTDEC-NI. However the optical depth shows large differences between non-interactive and interactive simulations (Fig. 2). In the non-interactive cases the bulk of the volcanic cloud is restricted between 30° N–90° N, while in the interactive cases the maximum of the cloud is found between the equator

and 60° N. Significantly less volcanic aerosol is transported across the equator in YESTJUN-NI and YESTDEC-NI. The optical depth does not exceed values $\tau_{0.5}>1$. south of 30° S. The largest deviations occur for the summer case (between YESTJUN and YESTJUN-NI), where the maximum optical depth is shifted northwards by about 30° in the Northern Hemisphere. In the Southern Hemisphere $\tau_{0.5}$ peak optical depth in the first four months after the eruption is about 5 times lower in the non interactive case than in the interactive one. As the volcanic cloud is much less dispersed in YESTJUN-NI and YESTDEC-NI than in YESTJUN and YESTDEC, the maximum optical depth with values $\tau_{0.5}>10$ is more than twice as large than in the interactive cases. Similar to the Pinatubo case, the aerosol induced heating leads to a more global spreading and to a pronounced southward transport. It is therefore important for all volcanic tracer studies to treat the aerosol interactively. In the following sections we will investigate the radiative forcing in more detail.

3.3 Radiative heating

The calculation of radiative forcing is sensitive to its definition (Stenchikov et al., 1998). Here, we consider the instantaneous radiative forcing by calling the radiation code twice in the model. Radiative heating and net radiative fluxes are estimated at every time step from the difference between the radiation calculations with and without volcanic aerosol. The instantaneous aerosol radiative forcing (vertical structure of the aerosol net heating rates) is insensitive to climate variations except in the regions with changed dense clouds (Stenchikov et al., 1998). Figure 3 shows the simulated zonal mean vertical cross sections of the total aerosol radiative heating and the aerosol mass mixing ratio in both experiments for one, three, six, nine and twelve months after the eruption. In general, both experiments show a similar anomaly pattern, slightly modified by the latitudinal shift of the volcanic aerosol and the different annual cycle. In the first six months after the eruption, aerosol induced positive heating rate anomalies of more than 0.8 K/day are found in the tropical region with maximum values of more than 1.6 K/day three months after the eruption. Above 25 hPa in the tropics, and above 100 hPa in mid-latitudes and Northern Hemisphere high latitudes, strong negative heating rate anomalies are depicted in the first half year after the eruption. Maximum negative heating anomalies are found three months after the eruption with values of more than -1.6 K/day in YESTJUN and -0.8 K/day in YESTDEC. The strong cooling tendencies at higher altitudes in the stratosphere result from the heating anomalies in the long wave radiation. This becomes clear by analyzing the heating rate anomalies in the solar (0.25–4 μm) and the terrestrial (4–250 μm) bands of the ECHAM radiation scheme separately. In Fig. 4 this is shown for YESTJUN. A similar picture is found for YESTDEC (not shown). In the solar part of the spectrum, which includes both the visible (0.25–0.68 μm) and the near infrared (0.68–4 μm), positive heating anomalies due to the absorption of near infrared are found where the bulk of the aerosol cloud is located. In the first half year after the eruption maximum values above 0.8 K/day are found. A slight cooling due to less absorption by water vapor can be depicted in the troposphere. For the long-wave radiation the zonal mean structure in the troposphere and lowermost stratosphere is determined by a net gain of energy and positive heating rate anomalies owing to enhanced absorption of longwave radiation. They are in the order of up to 1.6 K/d three months after the eruption in the aerosol containing layers and below the aerosol cloud. Above this region, a net loss of energy and reduced heating is calculated by the model because less terrestrial radiation reaches this altitude and the aerosol irradiates more into space. Thus, strong cooling tendencies appear with maximum values of -3.2 K/day three months after the eruption. This strong cooling effect weakens with decreasing aerosol density over time and it's position is shifted from the middle of the aerosol layer to the top of the volcanic cloud. The cooling also prevents the aerosol laden air from further rising. While the maximum of the volcanic cloud is located around 20 hPa one month after the eruption, it is found between 100 and 30 hPa half a year later due to gravitational settling of the aerosol.

The strong negative anomalies are in contrast to earlier Pinatubo simulations with much less dense aerosol (Stenchikov et al., 1998; Timmreck et al., 1999a; Ramachandran et al., 2000), where the total radiative heating anomalies are dominated by the solar effect. The maximum total net heating anomalies simulated for our model study are only about three to four times higher than for the Pinatubo case (with values from 0.3–0.4 K/day in the first months after the eruption) although the initial SO_2 mass is about a factor of 100 higher. Hence, the radiative forcing is coupled to aerosol density in a non-linear (damped) way.

3.4 Flux anomalies

In our simulation we determine the forcing by radiation calculations with and without volcanic aerosol. Thus, we neglect any stratospheric temperature perturbation in our radiative calculation which may modify the forcing. Figure 5 shows for both experiments changes of the zonal mean net radiative flux at the top of the atmosphere and at the surface. In the case of YESTJUN we find at the surface in the first half year a net radiative cooling of less than -16 W/m^2 between 60° S and 60° N and less than -32 W/m^2 in the subtropics. In YESTDEC, minimum values less than -32 W/m^2 are not as frequent as in YESTJUN, but values less than -16 W/m^2 are found up to 90° N in Northern Hemisphere summer. At polar latitudes the forcing is positive in winter. Then the absorption of terrestrial radiation during the polar night leads to a gain of radiative energy, while at lower latitudes the loss due to backscattering of shortwave radiation is dominant.

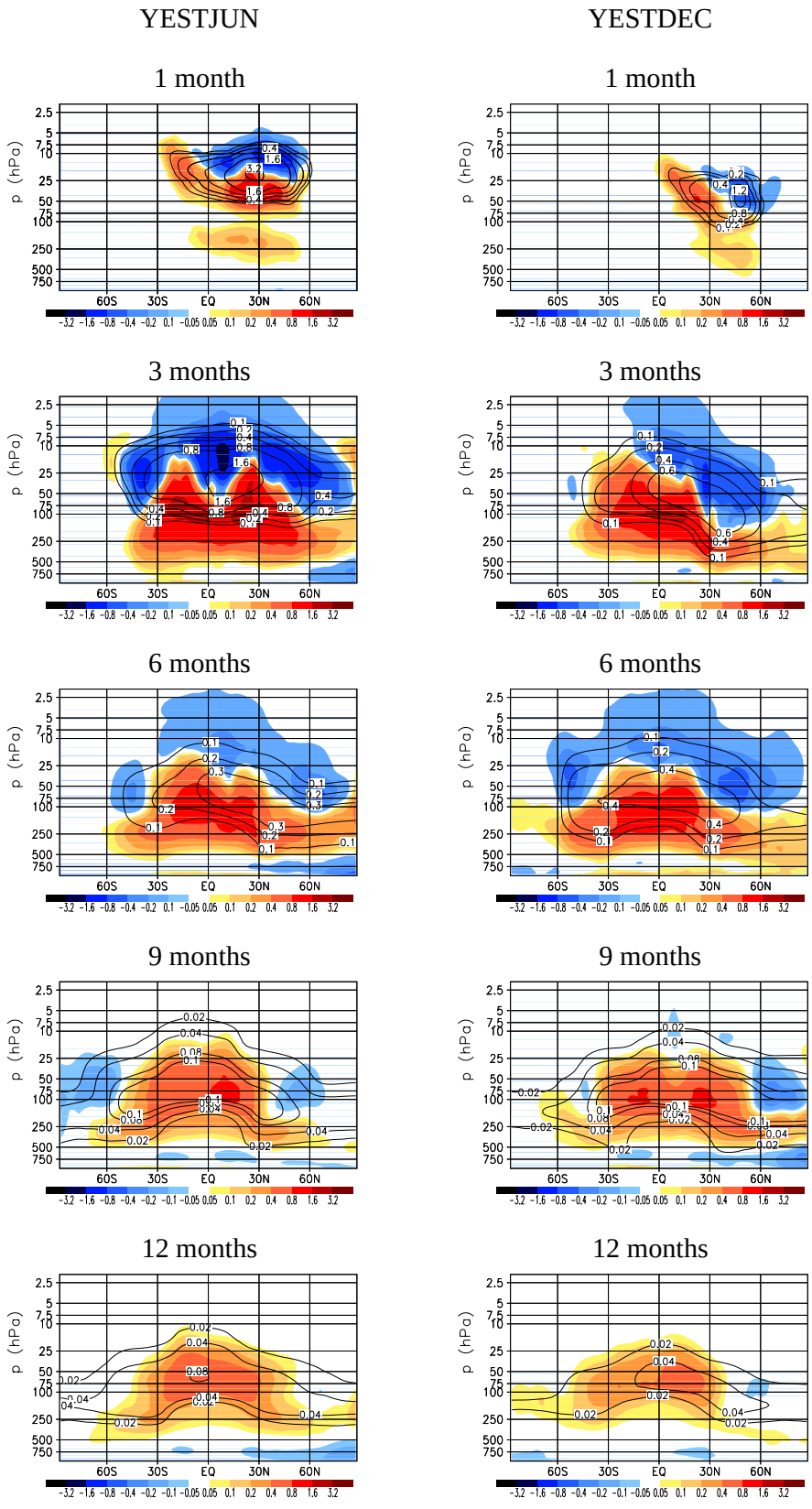

Fig. 3. Anomalies of the monthly mean zonally averaged total heating rates (K/d) caused by a theoretical super eruption in both experiments for different months after the eruption. The contour lines indicate the aerosol mass mixing ratio (ppm S).

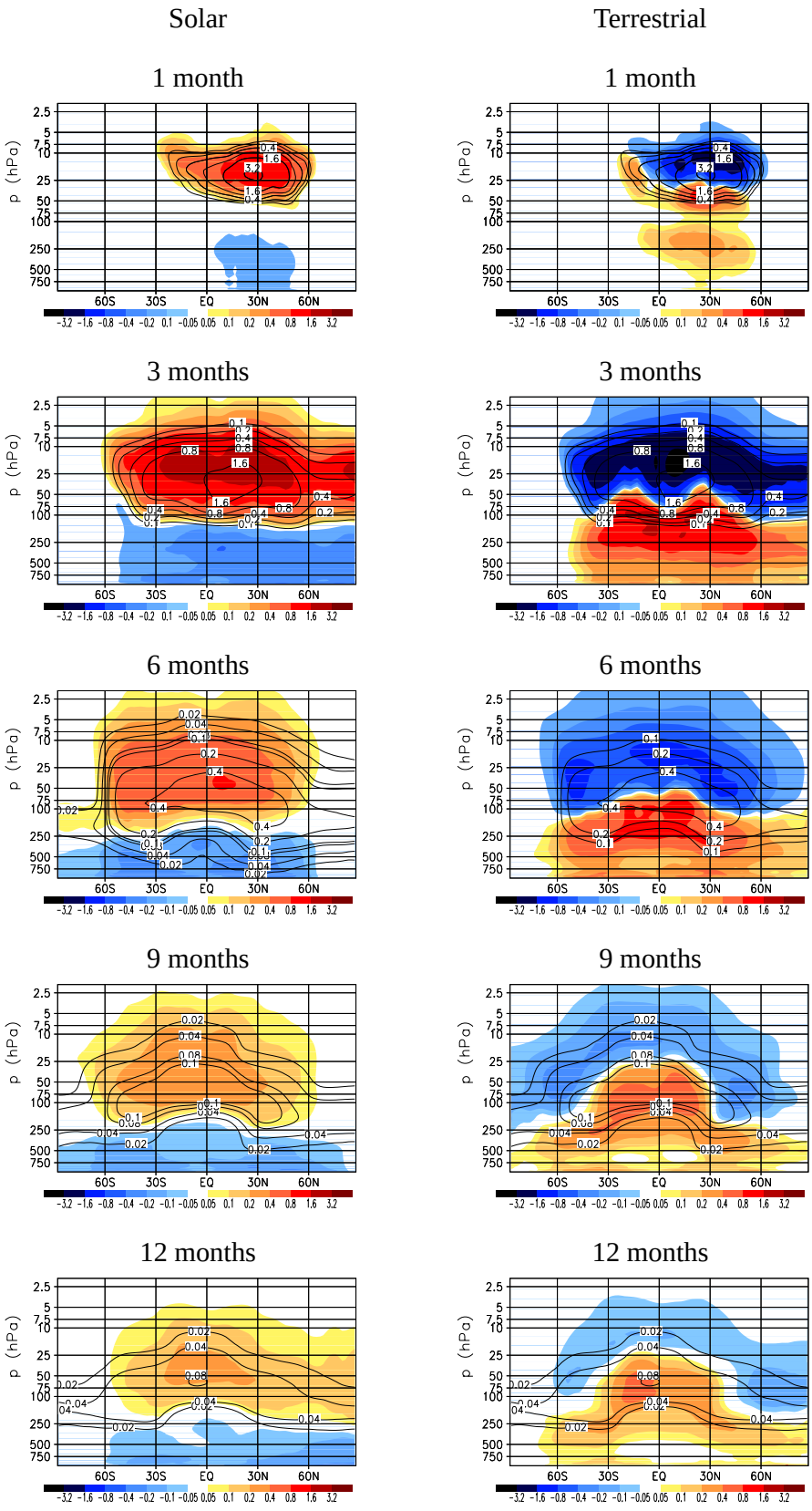

Fig. 4. Anomalies of the monthly mean zonally averaged solar (left panel) and terrestrial (right panel) heating rates (K/d) caused by a theoretical super eruption in YESTJUN for different months after the eruption. The contour lines indicate the aerosol mass mixing ratio (ppm S).

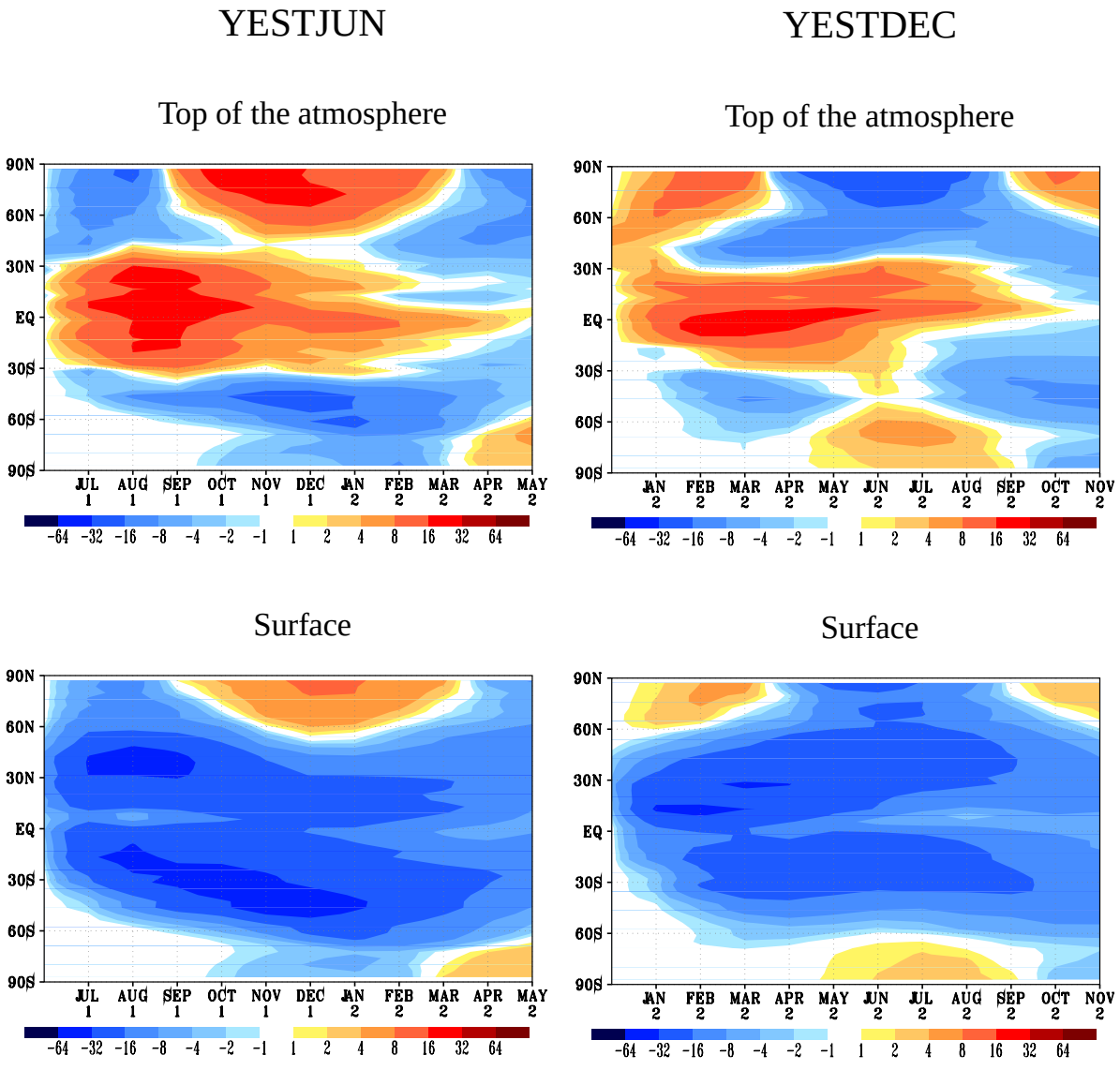

Fig. 5. Zonally and monthly averaged all–sky net radiative flux anomalies (W/m^2) between YESTJUN and a control run (left panel) and YESTDEC and a control run (right panel) at the top of the atmosphere and at the surface. Numbers at the abscissae indicate month after the eruption.

A comparison of the net radiative fluxes for the generic mid-latitude super eruption with the one calculated for the Pinatubo eruption shows that the structure of all-sky net radiative fluxes at the surface is similar, but about a factor of 6 larger. In contrast, the flux anomaly pattern at the top of the atmosphere is completely different in our study than for Pinatubo (Stenchikov et al., 1998) and Laacher See (Graf and Timmreck, 2001) eruptions. In addition to the positive flux anomalies in high latitudes during polar night, large positive flux anomalies of more than 16 W/m^2 are found in the first months after the eruption between 30° S and 30° N in YESTJUN and 10° S and 10° N in YESTDEC. The net gain of energy results from the strong positive flux anomalies in the long wave range due to the reduction of the outgoing long wave flux. This was also evident in the heating rates (Figs. 3, 4). Figure 6 shows for YESTJUN meridional cross sections of the net flux anomalies three and twelve months after the eruption for the total, the solar and the terrestrial part. The total net flux anomalies are dominated in the troposphere by changes in solar net flux, and in the tropical and subtropical stratosphere by changes in the long wave flux. The net flux anomaly in the solar spectrum is almost the same at all levels since the visible radiation is only scattered and not absorbed. Only in the region of high water vapor, clouds and volcanic aerosols modify the net flux as the near infrared radiation is absorbed by them. The net flux anomalies in the terrestrial

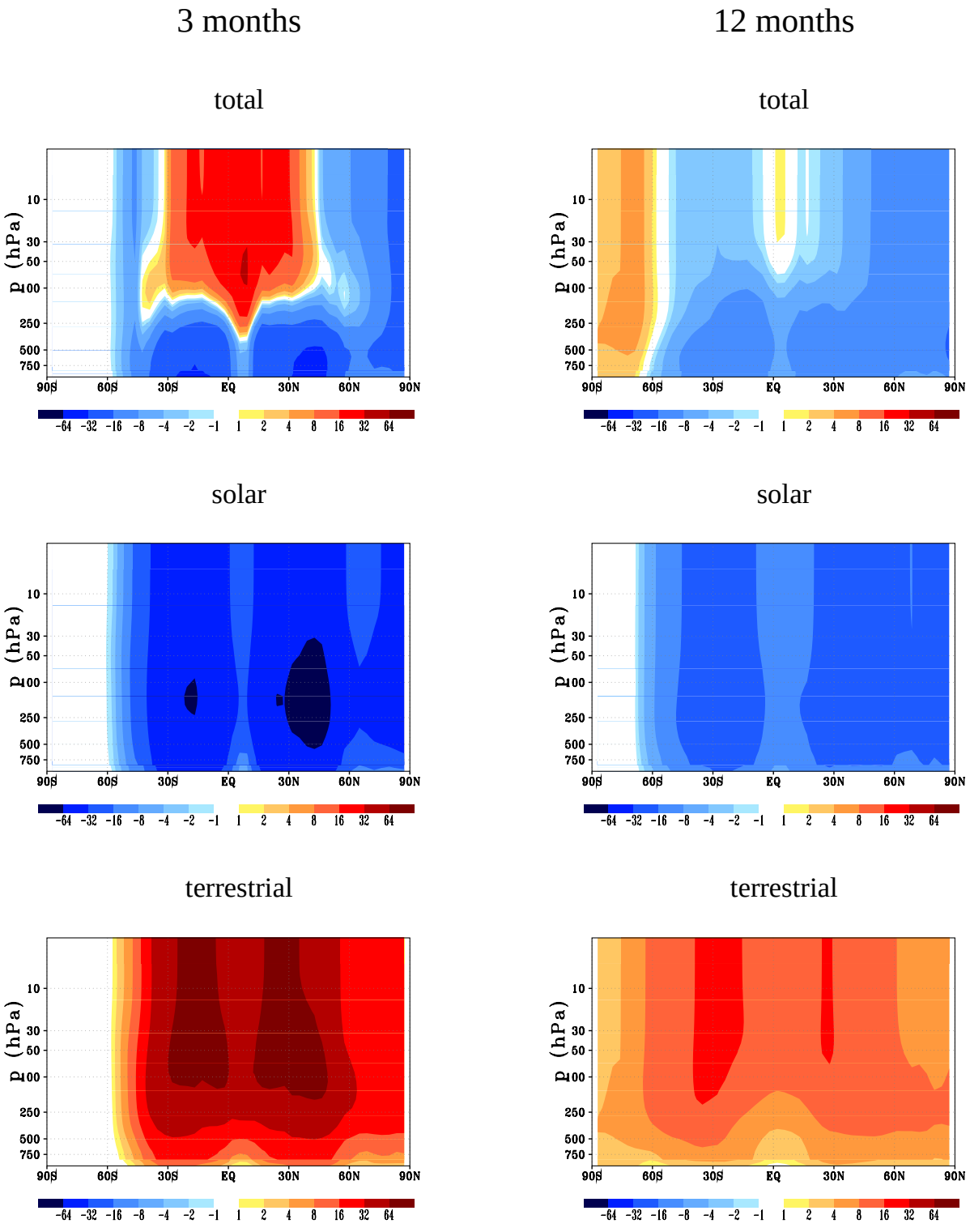

Fig. 6. Altitude-height cross section of monthly and zonally averaged radiative flux anomalies (W/m^2) between YESTJUN and a control run three and twelve months after the eruption.

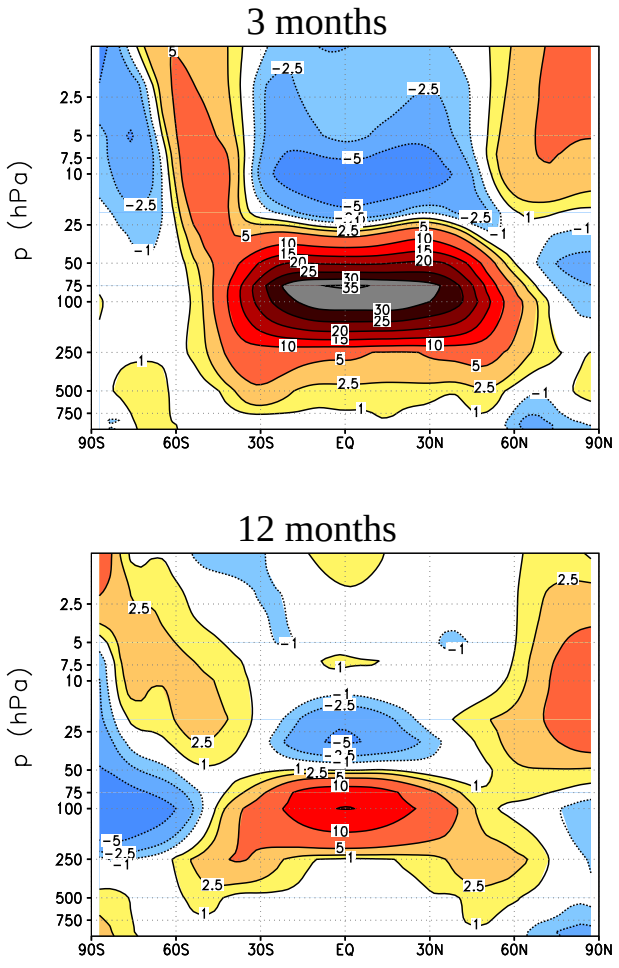

Fig. 7. Altitude-height cross section of monthly and zonally averaged temperature differences between YESTJUN and the control run.

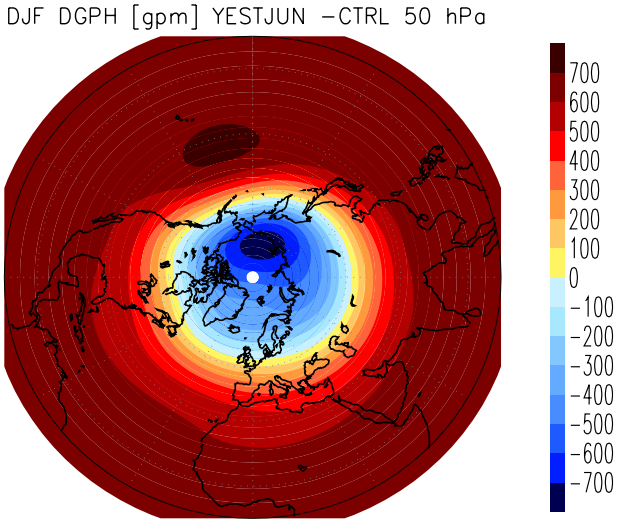

Fig. 8. Geopotential height anomalies [gpm] at 50 hPa between YESTJUN and the control run for the first winter after the eruption.

spectrum are steadily increasing with height. This is caused by the reduction of the outgoing thermal flux due to aerosol absorption.

3.5 Dynamical response

Our results are based on only one pair (disturbed and undisturbed) of numerical experiments. Hence, we concentrate on instantaneous radiative forcing rather than on climate sensitivity. Furthermore we have prescribed the SST. The runs are therefore not suitable to discuss possible climate effects of a Northern Hemisphere mid-latitude super eruption. However, a first comparison between the disturbed and the undisturbed model simulations revealed that very strong positive temperature anomalies of more than 30 K could be expected in the tropical lower stratosphere in the first months after the eruption. Negative temperature anomalies of several Kelvin due to the emission of longwave radiation were found above them. Figure 7 shows for YESTJUN the zonal averaged temperature anomalies three and twelve months after the eruption. Similar patterns can be seen for YESTDEC (not shown) but with slightly smaller negative and positve temperature anomalies due to less aerosol radiative heating (see also Fig. 3). Three months after the eruption maximum positive temperature anomalies of up to 35 K are found between 30° S and 30° N and between 75 hPa and 100 hPa. After one year the temperature anomaly in that region is still more than 10 K. Negative temperature anomalies are detected above 20 hPa with maximum values of more than −5 K around 10 hPa after three months. In the first year after the eruption the maximum height of the tropical cooling is slightly descending with time to 30 hPa and the spread of the negative temperature differences is also drastically reduced due to the vanishing longwave effect.

Stratospheric geopotential height and wind anomalies between the perturbed and the unperturbed run are similar to what one knows from large tropical eruptions e.g. Pinatubo (Graf et al., 1993; Timmreck et al., 1999b; Stenchikov et al., 2002, 2004). We see for YESTJUN that the strong pole-to-equator temperature gradient (Fig. 7) led to an enhanced polar vortex in the stratosphere (Fig. 8) in the first winter after the eruption (similar results we obtain for YESTDEC). This enhanced polar vortex strength will have effects on tropospheric climate via modulation of planetary wave propagation. However, in our simulations in the troposphere the temperature effect is only small and rapidly decreasing due to the prescribed SST.

To study tropospheric climate sensitivity a multi member ensemble run of a coupled ocean/atmosphere/chemistry model is necessary, which we are planning for the near future.

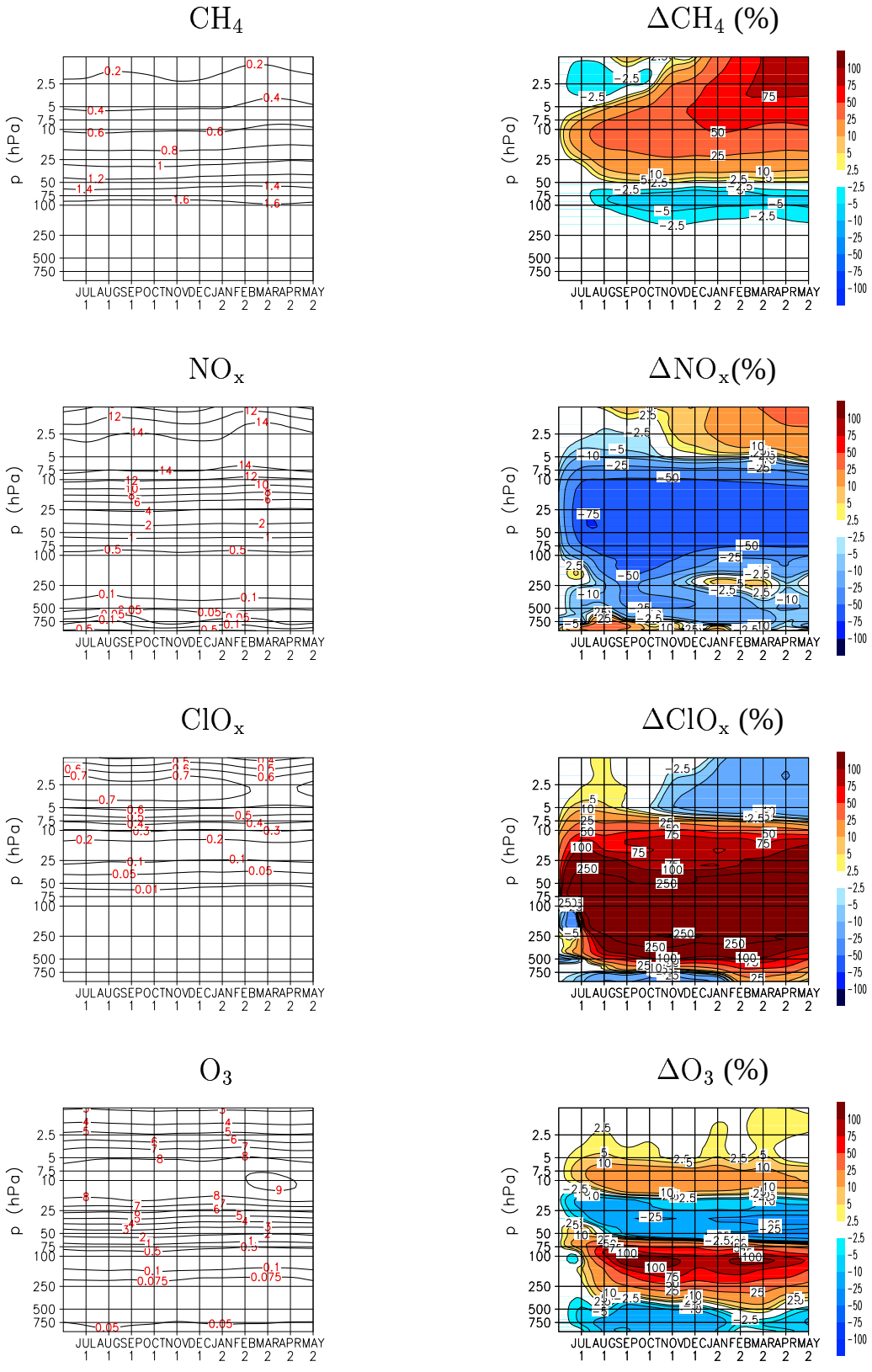

Fig. 9. Altitude-height cross section of the tropical averaged (30°S-30°N) trace gas concentrations in the control run and the simulated changes between the disturbed (YESTJUN) and the control run.

3.6 Chemical changes

Large Volcanic eruptions alter the chemical composition of the atmosphere significantly. It is therefore interesting to look at changes in the chemical concentration after such an eruption Our results are however limited because in the first months after the eruption, the high SO_2 concentration has a significant impact on stratospheric OH and O_3 (Bekki, 1995). This effect is not taken into account in the present simulation as well as the additional impact of volcanic released water vapor and halgon species are neglected. Figure 9 shows an altitude-height cross section of the average simulated tropical (30° S–30° N) changes in volume mixing ratio between the disturbed and the undisturbed run for YESTJUN. Analogous results are found for YESTDEC (not shown). The results in general look similar to what is known for trace gas changes after the Pinatubo eruption (Al-Saadi et al., 2001; Rozanov et al., 2002; Timmreck et al., 2003) but the deviations are much stronger. Aerosol induced heating leads to an uplift of the trace gases, which can clearly be seen in the upper stratospheric increase in CH_4 concentration of up to 75% and in the increase in NO_x above 40 km, The strong loss of more than 50% in the lower stratosphere in NO_x is mainly a result of heterogeneous chemistry. Heterogeneous reactions on the surface of the aerosol particles lead to a conversion of NO_x to HNO_3 and to chlorine activation (increase of ClO_x). The concentration of ClO_x increases by more than 250% in the aerosol containing layers and below, The tropical averaged O_3 mixing ratio decreases in our simulation between 20 km–30 km due to heterogeneous chemistry and upward transport (up to -20%), and increases above 30 km (up to 10%) due to a decrease in NO_x. This agrees qualitatively with other model studies (e.g. Rozanov et al. (2002)) and with measurements of tropical ozone profiles after Pinatubo (e.g. Grant et al. (2001)). While for the Pinatubo simulation we found only slight increases in the simulated O_3 mixing ratio below 20 km, the increase in O_3 is over 60% in our super volcano simulation in the first months after the eruption. This is probably due to changes in the photolysis rates. It should be emphazised that in the first months after the eruption, the high SO_2 loading has a significant impact on stratospheric OH and O_3 (Bekki, 1995). This effect is not taken into account in the present simulation and could modify the results in particular the O_3 concentration. Nevertheless the simulated changes are so strong that they should not be altered significantly when the resuced SO_2 loading is considered.

4 Conclusions

Simulating a Northern Hemisphere mid-latitude super eruption we forced a middle atmosphere chemistry climate model with an initial SO_2 cloud of 1700 Mt in the lower stratospheric mid-latitudes. Our experiments show that the dispersal of the volcanic cloud of a mid-latitude super eruption located at Yellowstone National Park is strongly dependent on the season of the eruption. The aerosol cloud of a summer eruption is transported west and more southward, while the cloud of a winter eruption is transported east and more northward. In the case of a summer eruption much more stratospheric aerosol is transported to the Southern Hemisphere. The reason for the seasonal dependent transport pattern is the stratospheric Aleutian high, which in the Northern Hemisphere summer months drives the volcanic cloud towards the equator. In boreal winter strong westerly winds are predominant which transport air east and northwards.

Optical thickness in the visible part of the solar spectrum reaches values above 10 during the first 6 months from northern tropics to mid-latitudes after the summer eruption, and in northern mid-latitudes after the winter eruption. If the aerosol is transported passively, the maximum optical thickness is strongly overestimated due to reduced meridional (southward) transport. A comparison of the net aerosol heating rate and flux anomalies for the generic Northern Hemisphere mid-latitude eruption with the one calculated for the Pinatubo eruption shows that the all-sky net radiative fluxes at the surface are about 6 times and the heating rate anomalies are about three to four times higher. Note that we used a 100fold initial sulphur injection! In contrast to prior studies of large volcanic eruptions of e.g. Mt Pinatubo size, our simulations revealed that the changes in the longwave radiation are dominant in the first months after the eruption, leading to strong cooling in the middle stratosphere and to large positive flux anomalies in the tropics and subtropics at the top of the atmosphere. At the surface we found large negative flux anomalies with peak values of less than $-32\,\mathrm{W/m^2}$. This will have important consequences for the climate effects, which will be studied in an upcoming investigation with a fully coupled ocean/atmosphere/chemistry model including dynamic vegetation. The simulation of a super eruption is however a quite difficult task due to the various complex interactions between chemical, microphysical, dynamical and biological processes. To understand the various feedback mechanisms it is important to investiagte them step by step. We suggest to start initially with an Atmosphere GCM studying the radiative and chemical effects of sulphate aerosol and ash. Furthermore the ash deposition at the surface and it's effect on albedo and snow cover will be included. In a second step the ocean response (SST, circulation changes due to altered atmospheric dynamics) should be investiged with a Atmosphere-Ocean GCM. Strong tropospheric cooling is expected in a fully coupled Atmosphere-Ocean GCM because of the large negative radiative flux anomalies at the surface. Massive negative temperature anomalies worldwide over several years would necessarily impact vegetation, especially tropical rain forests, and have at least a transient effect on the carbon and other biogeochemical cycles. It is therefore necessary to continue the work for a longer simulation period including the coupling with a dynamic vegetation model. Analyzing and understanding the climate effects of a

super eruption requires the full complexity of an Earth system model.

Acknowledgements. This work is partly supported by the German Science Foundation DFG grant TI 344/1-1 and by the European Commission under contract EVK2-CT-2001-000112 project PARTS. Computations were done at the Germann Climate Computer Center (DKRZ). The authors would like to thank M. Boettinger for preparing the movies and M. Giorgetta and H. Schmidt for valuable comments on an earlier version of this paper. The insightful reviews of S. Self, D. Stevenson and one anonymous reviewer are gratefully acknowledged.

Edited by: K. Hamilton

References

Al-Saadi, J., Pierce, R. B., Fairlie, T. D., et al.: Response of middle atmosphere chemistry and dynamics to volcanically elevated sulfate aerosol: Three-dimensional coupled model simulations, J. Geophys. Res., 106, 27 255–27 276, 2001.

Andronova, N. G., Rozanov, E. V., Yang, F., Schlesinger, M. E., and Stenchikov, G. L.: Radiative forcing by volcanic aerosols from 1850 through 1994, J. Geophys. Res., 104, 16 807–16 826, 1999.

Bekki, S.: Oxidation of volcanic SO_2: a sink for stratospheric OH and H_2O, Geophys. Res. Lett., 22, 913–916, 1995.

Bekki, S., Pyle, J. A., Zhong, W., Toumi, R., Haigh, J. D., und Pyle, D. M.: The role of microphysical and chemical processes in prolonging the climate forcing of the Toba eruption, Geophys. Res. Lett., 23, 2669–2672, 1996.

Christiansen, R. L.: The Quaternary and Pliocene Yellowstone Plateau volcanic field of Wyoming, Idaho, and Montana, U.S. Geological Survey Professional Paper, 729-G, 145 p.,2001.

Fairlie, T. D. A.: Three-dimensional transport simulations of the dispersal of volcanic aerosol from Mount Pinatubo, Q. J. R. Meteorol. Soc., 121, 1943–1980, 1995.

Feichter, J., Kjellström, E., Rodhe, H., Dentener, F., Lelieveld, J., and Roelofs, G.-J.: Simulation of the tropospheric sulfur cycle in a global climate model, Atmos. Environ., 30, 1693–1707, 1996.

Fouquart, Y., and Bonnel B.: Computations of solar heating of the earth atmosphere: A new parameterization, Contrib. Atmos. Phys., 53, 35–62, 1980.

Gates, W. L., Boyle, J. S., Covey, C., et al.: An Overview of the Results of the Atmospheric Model Intercomparison Project (AMIP I), Bull. Am. Met. Soc., 80, 29-55, 1999.

Graf, H.-F., Kirchner, I., Robock, A., and Schult, I.: Pinatubo eruption winter climate effects: Model versus observation, Clim. Dyn., 9, 81–93, 1993.

Graf, H.-F. and Timmreck, C.: A general climate model simulation of the aerosol radiative effects of the Laacher See eruption (10 900 BC), J. Geophys. Res., 106, 14 747–14 756, 2001.

Grant, W. B., Browell, E. V., Fishmann J., et al.: Aerosol-associated changes in tropical stratospheric ozone following the eruption of Mount Pinatubo, J. Geophys. Res., 99, 8197–8211, 1994.

Grainger, R. G., Lambert A., Rodgers, C. D., Taylor, F. W., Deshler, T.: Stratospheric aerosol effective radius, surface area and volume estimated from infrared measurements, J. Geophys. Res., 100, 16 507–16 518, 1995.

Hansen, J., Ruedy, R., and Sato, M.: Potential climate impact of Mount Pinatubo, Geophys. Res. Lett., 19, 215–218, 1992.

Kinne, S., Toon, O. B., and Prather, M. J.: Buffering of stratospheric circulation by changing amounts of tropical ozone: A Pinatubo case study, Geophys. Res. Lett., 19, 1927–1930, 1992.

Kirchner, I., Stenchikov, G. L., Graf, H.-F., Robock, A., and Antuna, J. C.: Climate model simulation of winter warming and summer cooling following the 1991 Mount Pinatubo eruption, J. Geophys. Res., 104, 19 039–19 055, 1999.

Lanphere, M. A., Champion, D. E., Christiansen, R. L., et al.: Revised ages for tuffs of the Yellowstone Plateau volcanic field: Assignment of the Huckleberry Ridge Tuff to a new geomagnetic polarity event, Geol. Soc. Am. Bull., 114, 559–568, 2002.

Manzini, E., Steil, B., Brühl, C., Giorgetta, M. A., and Krüger K.: A new interactive chemistry-climate model: 2. Sensitivity of the middle atmosphere to ozone depletion and increase in greenhouse gases and implications for recent stratospheric cooling, J. Geophys. Res., 108, 4429, doi:10.1029/2002JD002977, 2003.

Mason, B. G., Pyle, D. M., and Oppenheimer, C.: The size and frequency of the largest eruptions on Earth, Bull. Volcanol., 66, 735–748, 2004.

Morcrette, J. J.: Radiation and cloud radiative properties in the ECMWF operational weather forecast model, J. Geophys. Res., 96, 9121–9132, 1991.

Oppenheimer, C.: Limited global change due to the largest known Quaternary eruption, Toba 74 kyr BP?, Quaternary Science Reviews, 21, 1593–1609, 2002.

Pinto, J. R., Turco, R. P., and Toon, O. B.: Self-Limiting Physical and Chemical Effects in Volcanic Eruption Clouds, J. Geophys. Res., 94, 11 165–11 174, 1989.

Ramachandran, S., Ramaswamy, V., Stenchikov, G. L., and Robock, A.: Radiative impact of the Mount Pinatubo volcanic eruption: lower stratospheric response, J. Geophys. Res., 105, 24 409–24 429, 2000.

Rampino, M. R.: Supereruptions as a threat to civilizations on Earth-like planets, Icarus, 156, 562–569, 2002.

Roeckner, E., Arpe, K., Bengtsson, L., et al.,: The atmospheric general circulation model ECHAM-4: Model description and simulation of the present-day climate, Report 218, Max-Planck-Institut für Meteorologie, Hamburg, 1996.

Rozanov, E., Schlesinger, M. E., Andronova, N. G., et al.: Climate/Chemistry Effects of the Pinatubo volcanic eruption by the UIUC stratosphere/troposphere GCM with interactive photochemistry, J. Geophys. Res., 107, 4593, doi:10.1029/2001JD000974, 2002.

Sparks, R. S. J., Bursik, M. I., Carey, S. N., Gilbert, J. S., Glaze, L. S., Sigurdsson, H., and Woods, A. W.: Volcanic Plumes, John Wiley and Sons, Chichester, 1997.

Smith, R. B. and Siegel, L.: Windows into the Earth: The Geologic Story of Yellowstone and Grand Teton National Park: New York, Oxford University Press, p. 242, 2000.

Steil, B., Brühl, C., Manzini, E., et al.: A new interactive chemistry climate model, I- Present day climatology and interannual variability of the middle atmosphere using the model and 9 years of HALOE/UARS data, J. Geophys. Res., 108, 4290, doi:10.1029/2002JD002971, 2003.

Stenchikov, G. L., Kirchner, I., Robock, A., et al.: Radiative forcing from the 1991 Mt. Pinatubo volcanic eruption, J. Geophys. Res., 103, 13 837–13 858, 1998.

Stenchikov, G., Robock, A., Ramaswamy, V., Schwarzkopf, M. D., Hamilton, K., and Ramachandran, S.: Arctic Oscillation response to the 1991 Mount Pinatubo eruption: Effects of volcanic aerosols and ozone depletion, J. Geophys. Res., 107, 4803, doi:10.1029/2002JD002090, 2002.

Stenchikov, G., Hamilton, K., Robock, A., Ramaswamy, V., and Schwarzkopf, M. D.: Arctic Oscillation response to the 1991 Mount Pinatubo eruption in the SKYHI general circulation model with a realistic quai-biennial oscillation, J. Geophys. Res., 109, D03112, doi:10.1029/2003JD003699, 2004.

Timmreck, C., Graf, H.-F., and Feichter, J.: Simulation of Mt. Pinatubo aerosol with the Hamburg climate model ECHAM4, Theor. Appl. Climatol., 62, 85–106, 1999a.

Timmreck, C., Graf, H.-F., and Kirchner, I.: A one and a half year interactive simulation of Mt. Pinatubo aerosol, J. Geophys. Res., 104, 9337–9360, 1999b.

Timmreck, C.: Three-dimensional simulation of stratospheric background aerosol: First results of a multiannual GCM simulation, J. Geophys. Res., 106, 28 313–28 332, 2001.

Timmreck, C., Graf, H.-F., and Steil, B.: Aerosol chemistry interactions after the Mt. Pinatubo eruption, in: Volcanism and the Earth's Atmosphere, edited by: Robock, A. and Oppenheimer, C., AGU Monograph, 139, 214–225. 2003.

Young, R. E., Houben, H., and Toon, O. B.: Radiatively forced dispersion of the Mt. Pinatubo volcanic cloud and induced temperature perturbations in the stratosphere during the first few months following the eruption, Geophys. Res. Lett., 21, 369–372, 1994.

Yang, F., and Schlesinger M. E.: On the surface and atmospheric temperature changes followingthe 1991 Pinatubo volcanic eruption: A GCM study, J. Geophys. Res., 104, 9337–9360, 1999b.